ORIGINAL ARTICLE

lajss.org© Latin American Journal of Solids and Structures

www.lajss.org

Study on Scaled Model with Distortion of Free Vibration of Longitudinal Ring-Stiffened Large Thin-walled Cylindrical Shell

Ce Zheng[a], Yanguo Yang[b], Wei Yu[a,c]*, Shihao Chen[a], Lu Zhang[a,c], Shenghua Zhao[a,c]

[a] School of Civil Engineering, Guilin University of Technology, Guilin 541004, China. Email: zc18078498694@163.com, yuwei@glut.edu.cn, 1505637859@qq.com, 158792672@qq.com, 317785051@qq.com

[b] Tangshan iron and steel group CO. LTD, Tangshan, 063000, China. Email: yyg132@163.com

[c] Guangxi Key Laboratory of Green Building Materials and Construction Industrialization, Guilin University of Technology, Guilin, 541004, China. Email: yuwei@glut.edu.cn, 158792672@qq.com, 317785051@qq.com

*Corresponding author

https://doi.org/10.1590/1679-78258049

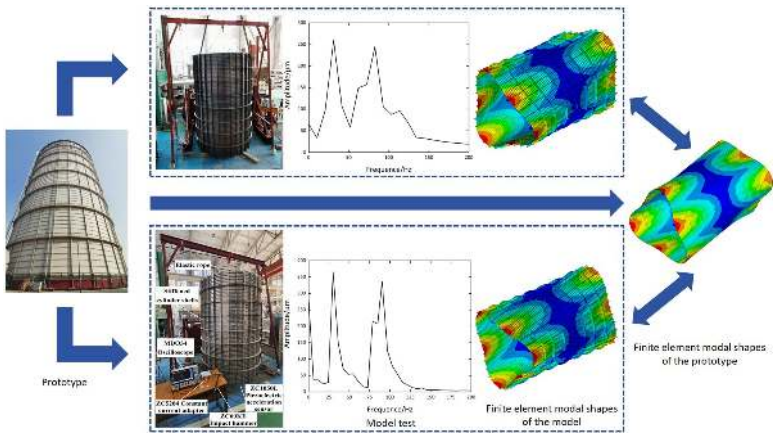
Abstract

For the design of scaled model and similarity prediction of vibration of 300,000m^3 blast furnace gasholder body, based on energy method and discrete stiffening theory, the scaling principle relation of gasholder body free vibration are derived. By using the thickness scale factor of the gasholder body skin and rib is distorted, and utilizing the stiffness equivalence, respectively, gasholder body scaled models (stiffened rib equivalent to rectangle) with geometric distortion and with both geometric and material distortion are designed and fabricated respectively. The free vibration of distortion similarity prediction of gasholder body prototype is carried out by the method of simulation and test. Results show that both two kinds of gasholder body scaled models, can predict the prototype frequency more accurately by using the similarity coefficient calculated by the average bending stiffness of column, ring rib, and wind-resistant ring. The proposed design method and scaling principle relation for gasholder body scaled model with free vibration and distortion are suitable for the design of scaled model distortion and similar prediction of free vibration of longitudinal ring-stiffened large thin-walled cylindrical shells with T-shaped and I-shaped stiffeners.

Keywords

stiffened cylindrical shell, energy method, discrete stiffening theory, free vibration, scaling principle

Graphical Abstract



Received: February 18, 2024. In revised form: April 14, 2024. Accepted: May 10, 2024. Available online: May 17, 2024.
https://doi.org/10.1590/1679-78258049

Latin American Journal of Solids and Structures. ISSN 1679-7825. Copyright © 2024. This is an Open Access article distributed under the terms of the Creative Commons Attribution License, which permits unrestricted use, distribution, and reproduction in any medium, provided the original work is properly cited.

1 INTRODUCTION

As a typical structural form of engineering structure, longitudinal ring-stiffened cylindrical shell is widely used in aerospace, submarine, petrochemical engineering, metallurgy, and other fields. The vibration problem of this type of longitudinal ring-stiffened large thin-walled cylindrical shells has attracted much attention. Because of the immense volume of the prototype structure, the vibration test of the prototype structure is subject to many limitations, such as high cost, long period, and difficulty. Currently, it is a common method to predict the vibration characteristics of prototype structures by using the test results of scaled model. Because the thickness of the skin and rib of the stiffened thin-walled shell is much smaller than that of other sizes, it is difficult to produce completely similar scaled models by using the existing materials and processing technologies. Therefore, in order to predict the vibration characteristics of the prototype through scaled model test, it is urgent to study the design method and scaling principle relation of scaled model with distortion for free vibration of longitudinal ring-stiffened large thin-walled cylindrical shell.

In recent years, many scholars have conducted in-depth research on the free vibration characteristics of stiffened cylindrical shells. Rinehart and Wang (1972) adopted the energy method to study the free vibration of longitudinal discrete stiffened cylindrical shells. Based on Donnell theory, the relationship between wave number and frequency of cylindrical shells with different number of stiffened ribs is studied by using Fourier series to represent the circumferential modal shapes and considering the sine wave forms in the longitudinal direction. Jafari and Bagheri (2006) used the energy method to analyze the free vibration of the stiffened ribs with unequal spacing and non-uniform eccentricity in a circumferential discrete stiffened cylindrical shell. Based on Love thin shell theory, Jam et al. (2012) studied the free vibration of reticulated stiffened cylindrical shells by Galerkin method, and derived the analytical solution of structural free vibration by using the equivalent stiffness model. Liu et al. (2013) simulated the arbitrary boundary constraints of orthogonal stiffened cylindrical shells by introducing artificial spring constraints and adjusting spring stiffness. They used the Gram-Schmidt orthogonalization method to establish characteristic orthogonal polynomials as the axial vibration mode function of the cylindrical shell, and used the Ritz method to derive the frequency equation of the cylindrical shell. Based on the transfer matrix method, Wang et al. (2018) studied the traveling wave resonance characteristics of thin-walled short cylindrical shells rotating in high speeds with circumferential grate teeth under different boundary conditions. They introduced the transfer matrix method and derived the transfer matrix relation of the whole structure from the state vectors between the shell subsegments. Liu et al. (2021) studied the modal frequency of the inner circumferentially stiffened functionally graded cylindrical shell, that is, using the Mori-Tanaka model and the third-order shear deformation theory, the energy model of structural free vibration is established, and the modal frequency equation of the stiffened functionally graded cylindrical shell is derived by combining the principle of minimum potential energy and the energy method. Niu et al. (2023) adopted the Novozhilov shell theory, considered the influence of translation and rotational inertia terms of the shells and longitudinal ribs, obtained the structural free vibration characteristic equation based on the energy method, established the dynamic analysis model of the free vibration of longitudinally stiffened cylindrical shells, and studied the influence of the position, number and eccentric distance of stiffened ribs on the natural frequency of longitudinally stiffened cylindrical shells. Most of the researchers mentioned in the above literature only studied the stiffened cylindrical shells with a single type of stiffened ribs, and there were few studies on the longitudinal ring-stiffened cylindrical shells.

In addition, using scaled models to predict the vibration characteristics of prototype structures is also one of the commonly used research methods. Torkamani et al. (2009) derived the similarity conditions for the free vibration of orthogonal stiffened cylindrical shells using similarity theory. They modeled the orthogonal stiffened cylindrical shells by considering geometric nonlinearity and dense stiffening theory, and conducted free vibration analysis using the principle of minimum potential energy. Yu and Li (2016) directly applied similarity transformation to the total energy of structural systems and derived generalized similarity conditions and scaling principle for the free vibration of orthogonal stiffened cylindrical plates and shells. By relaxing some similarity conditions, they designed a scaled model in which the material and geometric dimensions of the skin and stiffened rib are distorted. Also, they verified through numerical examples that the scaled model with distortion can accurately predict the vibration characteristics of the prototype. Luo et al. (2016) conducted research on the applicability of dynamic similarity models for thin-walled structures. Based on the governing equation, they derived the geometric distortion scaling law of typical thin-walled structures. Taking the thin-walled annular plate as an example, they put forward the accurate scaling law of the first five-order frequencies, and validated the effectiveness of similarity design methods through experiments. Zhou and Li (2019) proposed an equivalent similarity method, which simplified the governing equation by establishing an equivalent transition model, thereby simplifying the scaling principle and avoiding structural similarity distortion. They derived the equivalent criterion and scaling law that satisfy the equivalent similarity of the overall bending modes of the longitudinally stiffened cylindrical shells, and verified through numerical examples that the proposed equivalent similarity method can effectively solve the problem of

similarity distortion in the thickness and stiffened rib size of stiffened cylindrical shells. To sum up, it can be seen that most of the studies on scaled models focus on the scaling of geometric dimensions, and there are few studies on the predictive prototypes of scaled models of different materials.

In this paper, taking the 300,000m^3 blast furnace gasholder body as the research object, explored the distortion scaling principle of free vibration of longitudinal ring-stiffened large thin-walled cylindrical shells. Section 2 using the discrete stiffening theory and the total energy of the structural system, the generalized similarity conditions of free vibration of the gasholder body are derived. And section 3 obtained the scaling principle relation from the section 2. In section 4, by considering the geometric and material distortion of the scaled model, gasholder body scaled models (stiffened rib equivalent to rectangle) with geometric distortion and with both geometric and material distortion are designed and fabricated respectively. The finite element (FEM) and test methods are used to analyze the free vibration of the gasholder body. Section 5 used the finite element and test results of the section 4 are combined with the derived scaling principle relation in the section 3, the distortion similarity prediction of gasholder body free vibration is carried out to verify the accuracy of the design method and scaling principle relation for gasholder body scaled model with free vibration and distortion.

2 GENERALIZED SIMILARITY CONDITIONS FOR FREE VIBRATION OF LONGITUDINAL RING-STIFFENED CYLINDRICAL SHELL BASED ON ENERGY METHOD

In the process of similarity analysis, mathematical models of similar structural systems shall be the same. Therefore, the relationship between the total energy of any two similar structural systems can be expressed by the following (Ungbhakorn and Singhatanadgid, 2009):

$$\Pi_{\mathrm{p}}\left(X_{\mathrm{p}i}\right)=\psi\left(C_i\right)\Pi_{\mathrm{m}}\left(X_{\mathrm{m}i}\right) \tag{1}$$

Where, subscripts p and m represent the prototype and scaled model, respectively; $X_{\mathrm{p}i}$ and $X_{\mathrm{m}i}$ (i=1,2,…,n) represent the geometric and material parameters of the prototype and scaled model, respectively; Π represents the total energy of the structural system; $\psi(C_i)$ (i=1,2,…,n) represents the similarity function of two structural parameters. According to the similarity relation (1) of total energy, the generalized similarity conditions and scaling principle relation of structural vibration can be derived.

The 300,000m^3 blast furnace gasholder is as shown in Fig 1, and the gasholder body column, ring rib, and equivalent wind-resistant ring are as shown in Fig 2.

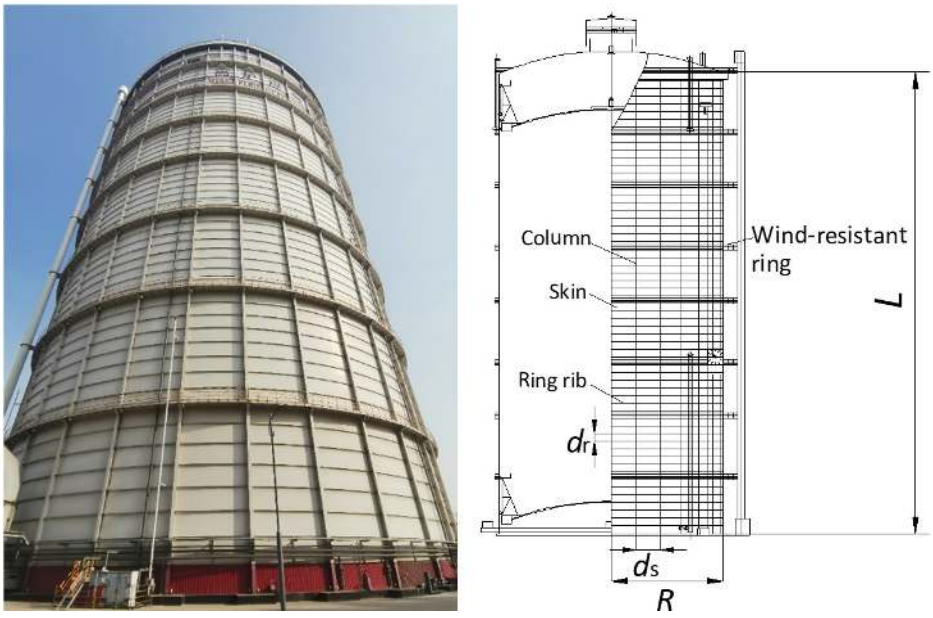


Fig 1. 300,000m^3 blast furnace gasholder.

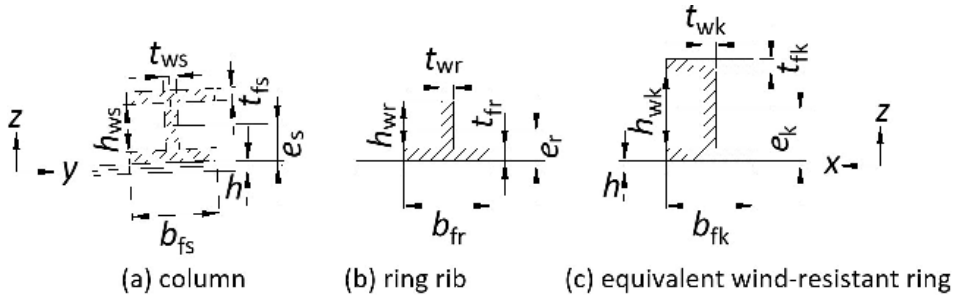


Fig 2. Configurations of the gasholder body column, ring rib and equivalent wind-resistant ring.

In Fig 1 and Fig 2, *R* represents the radius of the gasholder body skin, *L* represents the height of the gasholder body, and *h* represents the thickness of the gasholder body skin. Subscripts s, r, and k represent column, ring rib, and wind-resistant ring, respectively. d_s and d_r respectively represent the spacing between two adjacent columns and circumferential stiffened ribs, where the distance from the wind-resistant ring to the adjacent ring rib is equal to the spacing between the ring ribs. b_{fs}, t_{fs} and h_{ws}, t_{ws} respectively represent the length and thickness of the flange and web of the I-shaped column. b_{fr}, t_{fr} and h_{wr}, t_{wr} respectively represent the length and thickness of the flange and web of the T-shaped ring rib. b_{fk}, t_{fk} and h_{wk}, t_{wk} respectively represent the length and thickness of the equivalent I-shaped wind-resistant ring flange and web.

The energy functional of the longitudinal ring-stiffened cylindrical gasholder body can be expressed as:

$$\Pi = U + T_{\max} \tag{2}$$

Where: *U* and T_{max} are the strain energy and maximum kinetic energy of the gasholder body, respectively.

Based on Donnell's assumption, the linear geometric equation of the middle surface of the gasholder body skin is (Egle and Sewall, 1968; Amabili, 2008):

$$\begin{aligned} &\varepsilon_x = \frac{\partial u}{\partial x}, \varepsilon_y = \frac{\partial v}{\partial y} + \frac{w}{R}, \gamma_{xy} = \frac{\partial u}{\partial y} + \frac{\partial v}{\partial x} \\ &\chi_x = -\frac{\partial^2 w}{\partial x^2}, \chi_y = -\frac{\partial^2 w}{\partial y^2}, \chi_{xy} = -\frac{\partial^2 w}{\partial x \partial y} \end{aligned} \tag{3}$$

Where: *u, v, w* are respectively the longitudinal, circumferential, and radial displacement of the gasholder body skin.

The Institute of Mechanics, Chinese Academy of Sciences, Group of Solid Mechanics Research Shell proposed in Stiffened cylindrical panels and cylindrical shells (1983), the linear geometric equation of stiffened rib is:

$$\varepsilon_{x_s} = \varepsilon_x - e_s \frac{\partial^2 w}{\partial x^2}, \varepsilon_{y_r} = \varepsilon_y - e_r \frac{\partial^2 w}{\partial y^2}, \varepsilon_{y_k} = \varepsilon_y - e_k \frac{\partial^2 w}{\partial y^2} \tag{4}$$

Where: *e* is the distance from the centroid of the stiffened rib to the middle surface of the skin.

Based on the discrete stiffening theory, the internal force expression of the gasholder body skin is (Li et al. 2022):

$$\begin{aligned} &N_x = B\left(\varepsilon_x + \mu\varepsilon_y\right), N_y = B\left(\varepsilon_y + \mu\varepsilon_x\right), \\ &N_{xy} = Gh\gamma_{xy}, M_x = D\left(\chi_x + \mu\chi_y\right), \\ &M_y = D\left(\chi_y + \mu\chi_x\right), M_{xy} = D\left(1-\mu\right)\chi_{xy} \end{aligned} \tag{5}$$

Where: N_x, N_y, and N_{xy} are the stress resultants in the corresponding directions per unit length of the gasholder body skin, respectively; M_x, M_y, and M_{xy} are the bending moments resultants per unit length of the gasholder body skin, respectively; ε_x, ε_y, and γ_{xy} are the strains in the middle surface of the gasholder body skin; χ_x, χ_y, and χ_{xy} represent the curvatures of the gasholder body skin; μ is the Poisson's ratio of the skin material; *B*, *D*, and *G* are respectively the extensional rigidity, bending rigidity, and shear modulus of skin, which are expressed as:

$$B = \frac{Eh}{1-\mu^2}, D = \frac{Eh^3}{12\left(1-\mu^2\right)}, G = \frac{E}{2\left(1+\mu\right)} \tag{6}$$

Where, E is the elastic modulus of the skin.

In order to obtain a detailed expression of the total energy of the longitudinal ring-stiffened cylindrical gasholder body, the strain energy expressions of the skin and stiffened rib are introduced (Institute of Mechanics, Chinese Academy of Sciences, Group of Solid Mechanics Research Shell, 1983; Fisher, 1972):

$$\begin{aligned}
U_{\mathrm{c}} &= \frac{1}{2}\int_0^{2\pi R}\int_0^{L}\begin{pmatrix} N_x\varepsilon_x + N_y\varepsilon_y + N_{xy}\gamma_{xy} - M_x\dfrac{\partial^2 w}{\partial x^2} \\ -M_y\dfrac{\partial^2 w}{\partial y^2} - 2M_{xy}\dfrac{\partial^2 w}{\partial x\partial y}\end{pmatrix}dxdy \\
U_{\mathrm{s}} &= \frac{1}{2}\sum_{n_{\mathrm{s}}=1}^{N_{\mathrm{s}}}\left(\int_0^{2\pi R}\int_0^{L}\begin{pmatrix} E_{\mathrm{s}}A_{\mathrm{s}}\varepsilon_x^2 - 2E_{\mathrm{s}}A_{\mathrm{s}}e_{\mathrm{s}}\varepsilon_x\dfrac{\partial^2 w}{\partial x^2} + \\ E_{\mathrm{s}}I_{0\mathrm{s}}\left(\dfrac{\partial^2 w}{\partial x^2}\right)^2 + G_{\mathrm{s}}J_{\mathrm{s}}\left(\dfrac{\partial^2 w}{\partial x\partial y}\right)^2\end{pmatrix}\delta(y - n_{\mathrm{s}}d_{\mathrm{s}})dxdy\right) \\
U_{\mathrm{r}} &= \frac{1}{2}\sum_{n_{\mathrm{r}i}}^{N_{\mathrm{r}i}}\left(\int_0^{2\pi R}\int_0^{L}\begin{pmatrix} E_{\mathrm{r}}A_{\mathrm{r}}\varepsilon_y^2 - 2E_{\mathrm{r}}A_{\mathrm{r}}e_{\mathrm{r}}\varepsilon_y\dfrac{\partial^2 w}{\partial y^2} + \\ E_{\mathrm{r}}I_{0\mathrm{r}}\left(\dfrac{\partial^2 w}{\partial y^2}\right)^2 + G_{\mathrm{r}}J_{\mathrm{r}}\left(\dfrac{\partial^2 w}{\partial x\partial y}\right)^2\end{pmatrix}\delta(x - n_{\mathrm{r}i}d_{\mathrm{r}})dxdy\right) \\
U_{\mathrm{k}} &= \frac{1}{2}\sum_{n_{\mathrm{k}i}}^{N_{\mathrm{k}i}}\left(\int_0^{2\pi R}\int_0^{L}\begin{pmatrix} E_{\mathrm{k}}A_{\mathrm{k}}\varepsilon_y^2 - 2E_{\mathrm{k}}A_{\mathrm{k}}e_{\mathrm{k}}\varepsilon_y\dfrac{\partial^2 w}{\partial y^2} + \\ E_{\mathrm{k}}I_{0\mathrm{k}}\left(\dfrac{\partial^2 w}{\partial y^2}\right)^2 + G_{\mathrm{k}}J_{\mathrm{k}}\left(\dfrac{\partial^2 w}{\partial x\partial y}\right)^2\end{pmatrix}\delta(x - n_{\mathrm{k}i}d_{\mathrm{k}})dxdy\right)
\end{aligned} \tag{7}$$

Where: U_{c}, U_{s}, U_{r}, and U_{k} are the strain energies of the gasholder body skin, the longitudinally stiffened rib, the circumferentially stiffened rib, and the circumferential wind-resistant ring, respectively; e_{s}, e_{r}, and e_{k} are the distances from the centroid of the longitudinal rib section, the centroid of the ring rib section, and the centroid of the wind-resistant ring section to the middle surface of the skin, respectively; E_{s}, E_{r}, and E_{k} are the elastic moduli of longitudinal rib, ring rib, and wind-resistant ring, respectively; $I_{0\mathrm{s}}$, $I_{0\mathrm{r}}$, and $I_{0\mathrm{k}}$ are the moments of inertia from longitudinal rib, ring rib, and wind-resistant ring to the middle surface of the skin, respectively; A is the cross-sectional area of the stiffened rib; N is the number of stiffened ribs, with 7 wind-resistant rings. The gasholder body is divided into 8 sections, and the number of ring ribs between the wind-resistant rings from the bottom of the gasholder body is alternately 6 and 7, respectively. $n_{\mathrm{r}i}$, $N_{\mathrm{r}i}$, and $n_{\mathrm{k}i}$, $N_{\mathrm{k}i}$ respectively represent the starting and ending numbers of each ring rib and each wind-resistant ring in the gasholder body, and their data numbers are as shown in the following equation:

$$n_{\mathrm{r}i} = 1,8,16,23,31,38,46,53\ (i = 1,2,\cdots,8)$$

$$N_{\mathrm{r}i} = 6,14,21,29,36,44,51,59\ (i = 1,2,\cdots,8)$$

$$n_{\mathrm{k}i} = N_{\mathrm{k}i} = 7,15,22,30,37,45,52\ (i = 1,2,\cdots,7)$$

J_{s}, J_{r}, and J_{k} represent the torsion constants of the corresponding stiffened ribs, and their expression is (Chen, 2001):

$$J = \frac{1}{3}\sum_{i=1}^{n_0} b_i t_i^3 \tag{8}$$

Where, n_0 is the number of rectangular strips of the stiffened rib section, b is the long side of a rectangular strip section, and t is the short side of a rectangular strip section.

Ignoring the influence of in-plane inertia of the gasholder body, the maximum kinetic energy of the gasholder body skin and stiffened rib can be expressed as (Fisher, 1972):

$$
\begin{aligned}
T_{\mathrm{c}} &= \frac{1}{2}\rho h\Omega^2\int_0^{2\pi R}\int_0^{L} w^2 dxdy \\
T_{\mathrm{s}} &= \frac{1}{2}\rho_{\mathrm{s}}A_{\mathrm{s}}\Omega^2\sum_{n_{\mathrm{s}}=1}^{N_{\mathrm{s}}}\int_0^{2\pi R}\int_0^{L} w^2\delta\left(y-n_{\mathrm{s}}d_{\mathrm{s}}\right)dxdy \\
T_{\mathrm{r}} &= \frac{1}{2}\rho_{\mathrm{r}}A_{\mathrm{r}}\Omega^2\sum_{n_{\mathrm{r}i}}^{N_{\mathrm{r}i}}\int_0^{2\pi R}\int_0^{L} w^2\delta\left(x-n_{\mathrm{r}i}d_{\mathrm{r}}\right)dxdy \\
T_{\mathrm{k}} &= \frac{1}{2}\rho_{\mathrm{k}}A_{\mathrm{k}}\Omega^2\sum_{n_{\mathrm{k}i}}^{N_{\mathrm{k}i}}\int_0^{2\pi R}\int_0^{L} w^2\delta\left(x-n_{\mathrm{k}i}d_{\mathrm{r}}\right)dxdy
\end{aligned}
\tag{9}
$$

Where: ρ is the mass density per unit volume of the skin, ρ_{s}, ρ_{r}, and ρ_{k} represent the mass density per unit area of longitudinal rib, ring rib, and wind-resistant ring, respectively; Ω is the frequency of the structure.

Expressions for strain energy and kinetic energy of the gasholder body based on discrete stiffening theory are:

$$
\begin{aligned}
U &= U_{\mathrm{c}} + U_{\mathrm{s}} + U_{\mathrm{r}} + U_{\mathrm{k}} \\
T_{\max} &= T_{\mathrm{c}} + T_{\mathrm{s}} + T_{\mathrm{r}} + T_{\mathrm{k}}
\end{aligned}
\tag{10}
$$

First, substitute equations (3)~(6) into equation (7), and combine equations (8) and (9) to obtain the specific expression of equation (10). Then, bring the specific expression of equation (10) into equation (2) to obtain the total energy expression of the gasholder body free vibration:

$$
\begin{aligned}
\Pi = \frac{1}{2}\int_0^{2\pi R}\int_0^{L}&\left\{\begin{array}{l}
\dfrac{Eh}{1-\mu^2}\left[\mu\left(\dfrac{\partial v}{\partial y}+\dfrac{w}{R}\right)+\dfrac{\partial u}{\partial x}\right]\dfrac{\partial u}{\partial x}+ \\
\dfrac{Eh}{1-\mu^2}\left[\mu\dfrac{\partial u}{\partial x}+\dfrac{\partial v}{\partial y}+\dfrac{w}{R}\right]\left(\dfrac{\partial v}{\partial y}+\dfrac{w}{R}\right)+\dfrac{Eh}{2\left(1+\mu\right)}\left(\dfrac{\partial u}{\partial y}+\dfrac{\partial v}{\partial x}\right)+ \\
\dfrac{Eh^3}{12\left(1-\mu^2\right)}\left[\mu\dfrac{\partial^2 w}{\partial x^2}\dfrac{\partial^2 w}{\partial y^2}+\left(\dfrac{\partial^2 w}{\partial x^2}\right)^2\right]+ \\
\dfrac{Eh^3}{12\left(1-\mu^2\right)}\left[\mu\dfrac{\partial^2 w}{\partial x^2}\dfrac{\partial^2 w}{\partial y^2}+\left(\dfrac{\partial^2 w}{\partial y^2}\right)^2\right]+\dfrac{Eh^3}{6\left(1+\mu\right)}\left(\dfrac{\partial^2 w}{\partial x\partial y}\right)^2
\end{array}\right\}dxdy + \\
&\frac{1}{2}\sum_{n_{\mathrm{s}}=1}^{N_{\mathrm{s}}}\int_0^{2\pi R}\int_0^{L}\left[\begin{array}{l}
E_{\mathrm{s}}A_{\mathrm{s}}\left(\dfrac{\partial u}{\partial x}\right)^2+E_{\mathrm{s}}I_{0\mathrm{s}}\left(\dfrac{\partial^2 w}{\partial x^2}\right)^2- \\
2E_{\mathrm{s}}A_{\mathrm{s}}e_{\mathrm{s}}\dfrac{\partial u}{\partial x}\dfrac{\partial^2 w}{\partial x^2}+G_{\mathrm{s}}J_{\mathrm{s}}\left(\dfrac{\partial^2 w}{\partial x\partial y}\right)^2
\end{array}\right]\delta\left(y-n_{\mathrm{s}}d_{\mathrm{s}}\right)dxdy + \\
&\frac{1}{2}\sum_{n_{\mathrm{r}i}}^{N_{\mathrm{r}i}}\int_0^{2\pi R}\int_0^{L}\left[\begin{array}{l}
E_{\mathrm{r}}A_{\mathrm{r}}\left(\dfrac{\partial v}{\partial y}+\dfrac{w}{R}\right)^2+E_{\mathrm{r}}I_{0\mathrm{r}}\left(\dfrac{\partial^2 w}{\partial y^2}\right)^2- \\
2E_{\mathrm{r}}A_{\mathrm{r}}e_{\mathrm{r}}\left(\dfrac{\partial v}{\partial y}+\dfrac{w}{R}\right)\dfrac{\partial^2 w}{\partial y^2}+G_{\mathrm{r}}J_{\mathrm{r}}\left(\dfrac{\partial^2 w}{\partial x\partial y}\right)^2
\end{array}\right]\delta\left(x-n_{\mathrm{r}i}d_{\mathrm{r}}\right)dxdy + \\
&\frac{1}{2}\sum_{n_{\mathrm{k}i}}^{N_{\mathrm{k}i}}\int_0^{2\pi R}\int_0^{L}\left[\begin{array}{l}
E_{\mathrm{k}}A_{\mathrm{k}}\left(\dfrac{\partial v}{\partial y}+\dfrac{w}{R}\right)^2+E_{\mathrm{k}}I_{0\mathrm{k}}\left(\dfrac{\partial^2 w}{\partial y^2}\right)^2- \\
2E_{\mathrm{k}}A_{\mathrm{k}}e_{\mathrm{k}}\left(\dfrac{\partial v}{\partial y}+\dfrac{w}{R}\right)\dfrac{\partial^2 w}{\partial y^2}+G_{\mathrm{k}}J_{\mathrm{k}}\left(\dfrac{\partial^2 w}{\partial x\partial y}\right)^2
\end{array}\right]\delta\left(x-n_{\mathrm{k}i}d_{\mathrm{r}}\right)dxdy + \\
&\frac{1}{2}\int_0^{2\pi R}\int_0^{L}\rho h\omega^2 w^2 dxdy+\frac{1}{2}\sum_{n_{\mathrm{s}}=1}^{N_{\mathrm{s}}}\int_0^{2\pi R}\int_0^{L}\rho_{\mathrm{s}}A_{\mathrm{s}}\omega^2 w^2\delta\left(y-n_{\mathrm{s}}d_{\mathrm{s}}\right)dxdy + \\
&\frac{1}{2}\sum_{n_{\mathrm{r}i}}^{N_{\mathrm{r}i}}\int_0^{2\pi R}\int_0^{L}\rho_{\mathrm{r}}A_{\mathrm{r}}\omega^2 w^2\delta\left(x-n_{\mathrm{r}i}d_{\mathrm{r}}\right)dxdy+\frac{1}{2}\sum_{n_{\mathrm{k}i}}^{N_{\mathrm{k}i}}\int_0^{2\pi R}\int_0^{L}\rho_{\mathrm{k}}A_{\mathrm{k}}\omega^2 w^2\delta\left(x-n_{\mathrm{k}i}d_{\mathrm{r}}\right)dxdy
\end{aligned}
\tag{11}
$$

The total energy expression (Eq. (11)) may be written for model and prototype. By introducing scale factor C_X, the structural variable of the prototype X_{p} can be represented by structural variable of the model X_{m} and the scaling factor C_X :

$$X_{\mathrm{p}} = C_X X_{\mathrm{m}} \tag{12}$$

where subscripts m and p refer to model and prototype, respectively. X represents any variables in the gasholder body, such as displacement, geometric size, physical properties, etc.

The similarity condition between model and prototype is to substitute the $C_X X_{\mathrm{m}}$ in eq. (12) into the energy expression of the prototype, and assuming $C_x = C_y = C_R$, using $\delta(ax) = \delta(x)/|a|$ (Cohen T.C et al. 1977), where a denotes C_x、C_y、C_{dr} and C_{ds} in this paper, by comparing the rewritten prototype energy expression with model energy expression, eliminate the same item, the generalized similarity conditions that need to be satisfied for complete similarity between model and prototype can be obtained:

$$C_{e_{\mathrm{s}}} = C_{e_{\mathrm{r}}} = C_{e_{\mathrm{k}}} = C_{d_{\mathrm{s}}} = C_{d_{\mathrm{r}}} = C_R \tag{13-1}$$

$$\begin{aligned} C_\rho C_h C_\Omega^2 &= C_{\rho_{\mathrm{s}}} C_{A_{\mathrm{s}}} C_\Omega^2 = C_{\rho_{\mathrm{r}}} C_{A_{\mathrm{r}}} C_\Omega^2 = C_{\rho_{\mathrm{k}}} C_{A_{\mathrm{k}}} C_\Omega^2 \\ &= \frac{C_E C_h C_\mu}{C_R^2} = \frac{C_E C_h}{C_R^2} = \frac{C_{A_{\mathrm{s}}} C_{E_{\mathrm{s}}}}{C_R^2} = \frac{C_{A_{\mathrm{r}}} C_{E_{\mathrm{r}}}}{C_R^2} = \frac{C_{A_{\mathrm{k}}} C_{E_{\mathrm{k}}}}{C_R^2} \\ &= \frac{C_{A_{\mathrm{s}}} C_{E_{\mathrm{s}}} C_{e_{\mathrm{s}}}}{C_R^3} = \frac{C_{A_{\mathrm{r}}} C_{E_{\mathrm{r}}} C_{e_{\mathrm{r}}}}{C_R^3} = \frac{C_{A_{\mathrm{k}}} C_{E_{\mathrm{k}}} C_{e_{\mathrm{k}}}}{C_R^3} \\ &= \frac{C_E C_h^3}{C_R^4} = \frac{C_{G_{\mathrm{s}}} C_{J_{\mathrm{s}}}}{C_R^4} = \frac{C_{G_{\mathrm{r}}} C_{J_{\mathrm{r}}}}{C_R^4} = \frac{C_{G_{\mathrm{k}}} C_{J_{\mathrm{k}}}}{C_R^4} = \frac{C_{E_{\mathrm{s}}} C_{I_{0\mathrm{s}}}}{C_R^4} = \frac{C_{E_{\mathrm{r}}} C_{I_{0\mathrm{r}}}}{C_R^4} = \frac{C_{E_{\mathrm{k}}} C_{I_{0\mathrm{k}}}}{C_R^4} \end{aligned} \tag{13-2}$$

Based on equation (13), further derive the necessary similarity conditions for perfectly scale that the model and prototype need to satisfy:

$$C_\rho C_h = C_{\rho_{\mathrm{r}}} C_{A_{\mathrm{r}}} = C_{\rho_{\mathrm{s}}} C_{A_{\mathrm{s}}} = C_{\rho_{\mathrm{k}}} C_{A_{\mathrm{k}}} \tag{14-1}$$

$$C_\mu = 1 \tag{14-2}$$

$$\begin{aligned} C_E C_h &= C_{A_{\mathrm{s}}} C_{E_{\mathrm{s}}} = C_{A_{\mathrm{r}}} C_{E_{\mathrm{r}}} = C_{A_{\mathrm{k}}} C_{E_{\mathrm{k}}} \\ &= \frac{C_{A_{\mathrm{s}}} C_{E_{\mathrm{s}}} C_{e_{\mathrm{s}}}}{C_R} = \frac{C_{A_{\mathrm{r}}} C_{E_{\mathrm{r}}} C_{e_{\mathrm{r}}}}{C_R} = \frac{C_{A_{\mathrm{k}}} C_{E_{\mathrm{k}}} C_{e_{\mathrm{k}}}}{C_R} \\ &= \frac{C_{G_{\mathrm{s}}} C_{J_{\mathrm{s}}}}{C_R^2} = \frac{C_{G_{\mathrm{r}}} C_{J_{\mathrm{r}}}}{C_R^2} = \frac{C_{G_{\mathrm{k}}} C_{J_{\mathrm{k}}}}{C_R^2} = \frac{C_{E_{\mathrm{s}}} C_{I_{0\mathrm{s}}}}{C_R^2} = \frac{C_{E_{\mathrm{r}}} C_{I_{0\mathrm{r}}}}{C_R^2} = \frac{C_{E_{\mathrm{k}}} C_{I_{0\mathrm{k}}}}{C_R^2} \end{aligned} \tag{14-3}$$

3 SCALING PRINCIPLE RELATION FOR THE FREE VIBRATION OF LONGITUDINAL RING-STIFFENED CYLINDRICAL GASHOLDER BODY

When the longitudinal ring-stiffened cylindrical gasholder body is subject to free vibration, the similar invariant of the natural frequency of the gasholder body can be obtained by equation (13-2):

$$C_{\bar{M}} C_\Omega^2 C_R^4 \,/\, C_{\mathrm{sti}} = 1 \tag{15}$$

Where, $\bar{M}$ is the mass per unit area, and in case of complete similarity, the expression for $C_{\bar{M}}$ can be expressed as:

$$C_{\bar{M}} = C_\rho C_h \tag{16-1}$$

$$C_{\bar{M}} = C_{\rho_{\mathrm{s}}} C_{A_{\mathrm{s}}} \tag{16-2}$$

$$C_{\bar{M}} = C_{\rho_{\mathrm{r}}} C_{A_{\mathrm{r}}} \tag{16-3}$$

$$C_{\bar{M}} = C_{\rho_{\mathrm{k}}} C_{A_{\mathrm{k}}} \tag{16-4}$$

C_{sti} represents the scaling factor of stiffness. In case of complete similarity, the specific expression of C_{sti} can be expressed as:

$$C_{\mathrm{sti}} = C_E C_h C_R^2 = C_E C_h^3 \tag{17-1}$$

$$C_{\mathrm{sti}} = C_{A_{\mathrm{s}}} C_{E_{\mathrm{s}}} C_R^2 = C_{A_{\mathrm{r}}} C_{E_{\mathrm{r}}} C_R^2 = C_{A_{\mathrm{k}}} C_{E_{\mathrm{k}}} C_R^2 \tag{17-2}$$

$$C_{\mathrm{sti}} = C_{A_{\mathrm{s}}} C_{E_{\mathrm{s}}} C_{e_{\mathrm{s}}} C_R = C_{A_{\mathrm{r}}} C_{E_{\mathrm{r}}} C_{e_{\mathrm{r}}} C_R = C_{A_{\mathrm{k}}} C_{E_{\mathrm{k}}} C_{e_{\mathrm{k}}} C_R \tag{17-3}$$

$$C_{\mathrm{sti}} = C_{G_{\mathrm{s}}} C_{J_{\mathrm{s}}} = C_{G_{\mathrm{r}}} C_{J_{\mathrm{r}}} = C_{G_{\mathrm{k}}} C_{J_{\mathrm{k}}} \tag{17-4}$$

$$C_{\mathrm{sti}} = C_{E_{\mathrm{s}}} C_{I_{0\mathrm{s}}} = C_{E_{\mathrm{r}}} C_{I_{0\mathrm{r}}} = C_{E_{\mathrm{k}}} C_{I_{0\mathrm{k}}} \tag{17-5}$$

Because of the natural frequency $f = \Omega/(2\pi)$, the scaling relation of the natural frequency of the gasholder body can be expressed as follows:

$$f_{\mathrm{p}}^2 = f_{\mathrm{m}}^2 \frac{C_{\mathrm{sti}}}{C_{\bar{M}} C_R^4} \tag{18}$$

The scaling relationship of the natural frequency of the gasholder body is:

$$C_f = \left[C_{\mathrm{sti}} \,/\, \left(C_{\bar{M}} C_R^4 \right) \right]^{0.5} \tag{19}$$

To accurately predict the vibration modes of the gasholder body prototype, the similarity conditions between the vibration modes of the model and the prototype are:

$$C_m = C_n = 1 \tag{20}$$

Where: *m* and *n* respectively represent the number of half waves along the longitudinal direction of the cylindrical gasholder body and the number of full waves in the circumferential direction.

4 FREE VIBRATION TEST OF GASHOLDER BODY SCALED MODEL AND EXAMPLE VERIFICATION OF FREE VIBRATION OF LONGITUDINAL RING-STIFFENED CYLINDRICAL SHELL

4.1 Free vibration test of gasholder body scaled model

4.1.1 Design and processing of gasholder body scaled model with distortion

Two scale models were designed and fabricated for the real tests: one fabricated from iron and the other from aluminum alloy. Use the equal geometric scaling factor of the height and radius of the gasholder body, as well as the equal thickness scaling factor of the skin and rib, a transition scale model is established firstly; And according to the equivalent tension-compression stiffness and bending stiffness of the stiffened ribs, the geometric distortion of the gasholder body scaled model is realized. On the basis of the gasholder body scaled model with geometric distortion, considering the material distortion of the scaled model, the new thickness dimensions of skin, column, ring rib, and wind-

resistant ring are obtained by using the equivalent tension-compression stiffness and bending stiffness, and both geometric and material distortion of the gasholder body scaled model are realized. Gasholder body scaled models (stiffened rib equivalent to rectangle) with geometric distortion and with both geometric and material distortion are processed and fabricated respectively.

Based on laboratory conditions and existing material types, the scaling factor of height and radius of gasholder body are selected to be 40, and the scaling factor of thickness of skin and stiffened plate are 3.5 and 7/6. The material and geometric parameters of the gasholder body prototype, transition scale model, scaled models with geometric distortion and with both geometric and material distortion are as shown in Table 1, respectively. Gasholder body scaled models (stiffened rib equivalent to rectangle) with geometric distortion and with both geometric and material distortion are as shown in Fig 3 and Fig 4.

Table 1. Material and geometric parameters of the gasholder body prototype, transition scale model, scaled models with geometric distortion and with both geometric and material distortion.

Parameters	Prototypical values	Scaling factor	Transition scale model values	Scaled model with geometric distortion	Scaled model with both geometric and material distortion
L/m	108	40	2.7	2.7	2.7
R/m	32.3	40	0.8075	0.8075	0.8075
h/m	0.007	3.5	0.002	0.002	0.006
ρ/(kg/m^3)	7850	1	7850	7850	2750
μ	0.3	1	0.3	0.3	0.3
E/Pa	2.06×10^{11}	1	2.06×10^{11}	2.06×10^{11}	6.875×10^{10}
h_{ws}/m	0.452	40	0.0113	0.0471	0.04713
t_{ws}/m	0.011	3.5	0.00314	0.00237	0.00709
h_{wr}/m	0.111	40	0.002775	0.01344	0.01344
t_{wr}/m	0.007	3.5	0.002	0.00147	0.0044
h_{wk}/m	1.106	40	0.02765	0.075	0.075
t_{wk}/m	0.008	3.5	0.00229	0.00131	0.00393



Fig 3. Model of iron stiffened cylindrical shell.

4.1.2 Test suspension and testing system for gasholder body scaled model

The test system of the gasholder body scaled model is as shown in Fig 4. The test system consists of gasholder body model, suspension, and acquisition system. The gasholder body model is hung on the suspension by elastic rope to realize the free condition of the boundary between the two ends of the gasholder body scaled model. The acquisition system consists of oscilloscope, impact hammer, constant current adapter, and piezoelectric acceleration sensor.



Fig 4. Suspension and testing system for free vibration test.

4.1.3 Acquisition and analysis of test results on the free vibration of gasholder body scaled model

During the test, the normal excitation is applied to the gasholder body scaled model test-piece by an impact hammer to make it vibrate. The acceleration sensor located at the bottom of the test-piece collects the voltage signals generated by the vibration, and transmits the signals to the oscilloscope for conversion, display, and storage. The data after twice the time of action of the hammer is selected, the time domain curve is transformed by fast Fourier transform using MATLAB program to obtain the frequency domain curve of the free vibration of the gasholder body scaled model, so as to identify the natural frequency of the free vibration of the gasholder body scaled model. The time-domain and frequency-domain curves of the gasholder body scaled model with geometric distortion and the gasholder body scaled model with both geometric and material distortion are shown in Fig 5 and Fig 6, respectively. Because frequencies of the first several orders of the free vibration of a stiffened cylindrical shell dominate, in this paper, natural frequencies of the first three orders of the stiffened cylindrical shell are analyzed.

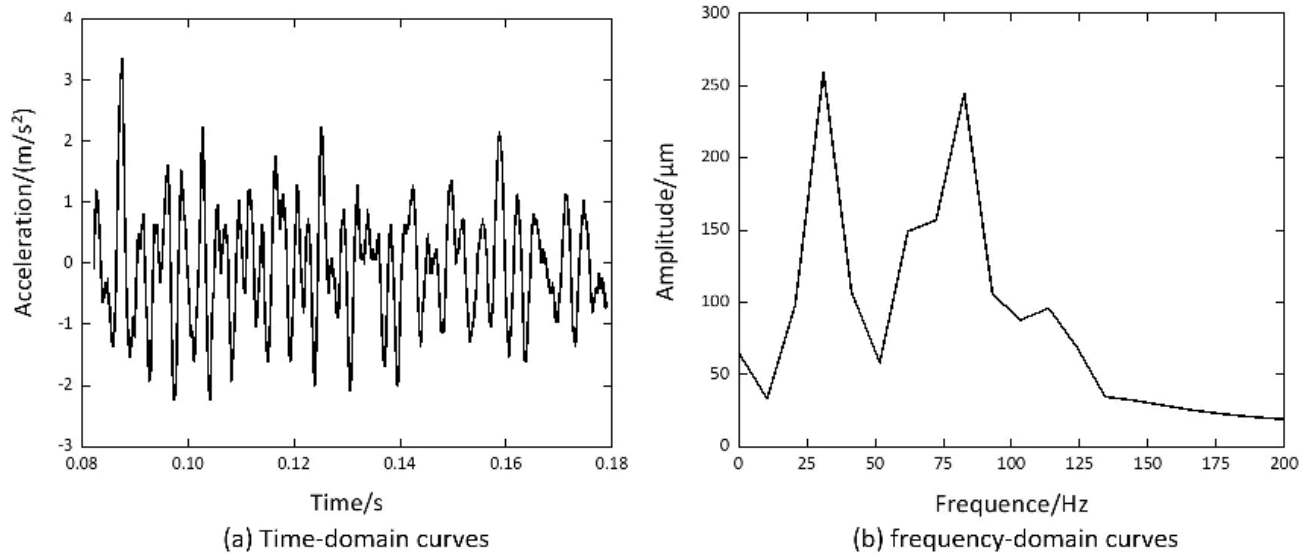


Fig 5. Time-domain and frequency-domain curves of the gasholder body scaled model with geometric distortion.

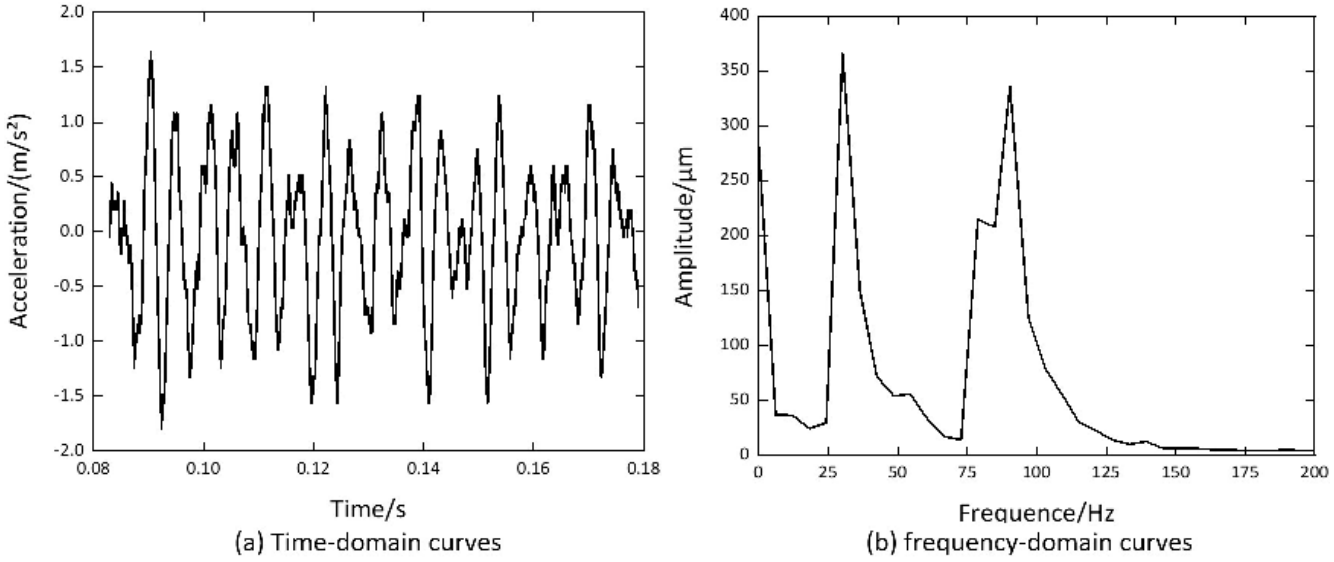


Fig 6. Time-domain and frequency-domain curves of the gasholder body scaled model with both geometric and material distortion.

4.2 Example verification of free vibration of longitudinal ring-stiffened cylindrical shell

Material and geometric parameters of longitudinally externally stiffened and circumferentially internally stiffened cylindrical shells in Literature (Mustafa and Ali 1989) are as follows: E=207GPa, μ=0.3, ρ=7430kg/m^3, L=0.813m, R=0.203m, h=0.00204m, h_{ws}=0.006m, t_{ws}=0.008m, h_{wr}=0.006m, t_{wr}=0.004m, N_r=13, N_s=20. A finite element model of the structure is established by using ANSYS software, and the shell 181 unit is used for the skin and stiffened rib. It can be seen from Table 2 that the free vibration frequency and vibration mode of the finite element analysis in this paper are in good agreement with the results of the literature.

Finite element free vibration analysis is conducted based on the parameters of the gasholder body scaled model test-pieces with geometric distortion and both geometric and material distortion. The skin of the prototype has 768 elements in the ring direction and 720 elements in the axial direction. The rib is reinforced by beam188 unit, which has the same number of elements as the skin in the ring direction. The model of iron and aluminum has the same elements number. The skin has 832 elements in the circumferential direction and 480 elements in the axial direction. In the radial direction, each ring rib has 3 elements, there are 6 elements between the ring rib and the column, and there are 5 elements between the column and the wind ring. The number of integration points in the shell element of the prototype and the model is 5, and their boundaries are free boundary conditions with not constrained.

The finite element analysis results and test results of the first-three-order vibrations of the two distortion models are compared respectively. The results are as shown in Table 3, and the errors are all within 5%. The accuracy of finite element analysis and the reliability of test results are verified.

Table 2. Comparison of free vibration characteristics of longitudinal ring-stiffened cylindrical shell.

Mode number (*m*,*n*)	Present the FEM result (Hz)	Ref. (Lee and Kim, 1998) (Hz)	Errors (%)	Ref. (Liu et al., 2016) (Hz)	Errors (%)	Ref. (Golchi et al., 2019) (Hz)	Errors (%)	Ref. (Mustafa and Ali, 1989) (Hz)	Errors (%)
(1,1)	925.64	951	-2.67	942	-1.74	939	-1.42	942	-1.74
(1,2)	450.94	458	-1.54	451	-0.01	441	2.25	439	2.72
(1,3)	343.79	350	-1.77	332	3.55	338	1.71	337	2.01
(1,4)	472.99	492	-3.86	473	-0.002	482	-1.87	482	-1.87
(1,5)	714.81	752	-4.95	737	-3.01	737	-3.01	740	-3.40

Note: Errors = (FEM result - results of the reference) / results of the reference.

Table 3. Comparison between finite element analysis and test results of free vibration of gasholder body scaled model.

Mode number (*m*,*n*)	the gasholder body scaled model only geometric distortion			the gasholder body scaled model with both material and geometric dimension distortion		
	Natural frequency calculated by FEM result (Hz)	Natural frequency calculated by vibration test result (Hz)	Errors (%)	Natural frequency calculated by FEM result (Hz)	Natural frequency calculated by vibration test result (Hz)	Errors (%)
(1,2)	30.549	30.985	-1.168	31.347	30.124	4.060
(1,2)	30.549	30.985	-1.168	31.347	30.124	4.060
(0,3)	35.793	-	-	36.361	-	-
(0,3)	35.793	-	-	36.361	-	-
(1,3)	84.639	82.628	2.434	86.866	90.371	-3.877
(1,3)	84.639	82.628	2.434	86.866	90.371	-3.877

Note: Errors = (FEM result- vibration test result) / vibration test result.

5 PREDICTION OF DISTORTION SIMILARITY IN FREE VIBRATION OF LONGITUDINAL RING-STIFFENED CYLINDRICAL GASHOLDER BODY

Because it is difficult to satisfy all the similarity conditions, it is not suitable to design and make exactly similar scaled models in practice. Therefore, some conditions of complete similarity can be ignored and the similarity of scaled model with distortion can be studied. In order to verify the correctness of the generalized similarity conditions and the scaling principle relation derived for the similarity of the gasholder body free vibration and distortion, first, Ansys finite element software is used to conduct free vibration simulation analysis on the gasholder body prototype. Second, the frequencies obtained from the simulation and test of the gasholder body scaled model are substituted into the scaling principle relation, and the two predictive frequencies of the gasholder body prototype are obtained. Finally, the two predictive frequencies of the gasholder body prototype are compared with the simulation frequencies of the gasholder body prototype, and the modal shapes of the corresponding free vibration order of the gasholder body scaled model and the prototype are judged to be consistent.

5.1 Free vibration similarity prediction with the same material and only geometric dimension distortion

Due to the thin thickness of the skin, column, ring rib, and equivalent wind-resistant ring of the gasholder body prototype, it is very difficult to produce a scaled model with complete similarity. Therefore, geometric distortion design of the scaled model is required. By using the finite element method and test method, and combined with the corresponding free vibration scaling principle relation, similarity prediction and analysis on the geometric distortion of the gasholder body free vibration is conducted.

Table 4. Similarity prediction of gasholder body free vibration with the same material and only geometric distortion.

Mode number (*m*,*n*)	Natural frequency calculated by FEM result for the prototype (Hz)	Natural frequency of prototype predicted by FEM result of scaled model (Hz)	Natural frequency of prototype predicted by vibration test result of scaled model (Hz)	Errors[1] (%)	Errors[2] (%)
(1,2)	0.275	0.276	0.280	0.501	1.936
(1,2)	0.275	0.276	0.280	0.501	1.936
(0,3)	0.324	0.323	-	-0.056	-
(0,3)	0.324	0.323	-	-0.056	-
(1,3)	0.764	0.766	0.748	0.227	-2.155
(1,3)	0.764	0.766	0.748	0.227	-2.155

Note: Errors[1] = (predicted by FEM results of scaled model - FEM result of prototype) / FEM result of prototype, Errors[2] = (predicted by vibration test results of scaled model - FEM result of prototype) / FEM result of prototype.

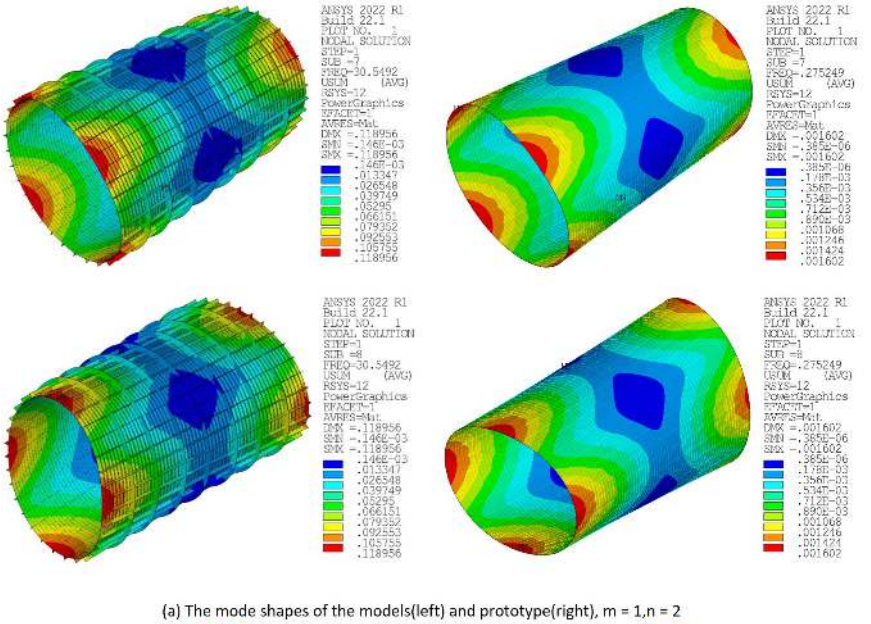
Table 4 presents the first-three-order modal wave numbers and natural frequencies of the free vibration finite element result of the gasholder body prototype, the prototype natural frequency predicted by combining the natural frequency of the scaled model with geometric distortion with the scaling principle equation (19), and the error in natural frequency of the predictive prototype and the prototype. Where, C_{sti} of the scaling relation (19) is taken as the scaling coefficient of the average bending stiffness of the column, ring rib, and wind-resistant ring in equation (17-5), that is, $C_{\mathrm{sti}} = C_{E_{\mathrm{average}}} C_{I_{0_{\mathrm{average}}}}$, so $C_{\mathrm{sti}} = 29241.709$; $C_{\bar{M}}$ is taken as the scaling coefficient of the average mass value of the column, ring rib, and wind-resistant ring in equations (16-2)~(16-4), and is calculated as $C_{\bar{M}} = 139.557$. Fig 7 shows the first-three-order model shape diagrams of the gasholder body scaled model with geometric distortion as calculated by finite element method and the gasholder body prototype. As can be seen from Table 4 and Fig 7, with only geometric distortion, the error between the finite element predicted natural frequency of the gasholder body prototype and the finite element result of the prototype is within 1%, and the finite element free vibration modal wave number of the gasholder body scaled model is consistent with that of the prototype; Because the free vibration test of the gasholder body scaled model with geometric distortion can not identify the second-order frequency, only the predicted values of the first- and third-order gasholder body prototype natural frequency tests are compared with the prototype finite element results, and the errors are 1.936% and -2.155%, respectively; The above results indicate that the free vibration characteristics of the gasholder body scaled model with only geometric dimension distortion, combined with the scaling principle relation (19) and relation (20), can well predict the free vibration characteristics of the gasholder body prototype, which fully verifies the correctness of the design method of the gasholder body scaled model with geometric distortion and the free vibration scaling principle relation.

Table 5 shows the error between the predicted first-order natural frequency of free vibration of the gasholder body scaled model with geometric distortion and the prototype finite element results when the coefficients in scaling principle relation (19) are calculated using the equations (16-1)~(16-4), the average values of equations (16-2)~(16-4) and the average values of equations (16), as well as the equations (17-1)~(17-5), the average values of equations (17) and (17-5), respectively. Due to the large number of value combinations, only the result with the smallest error in each group is given. By comparison, it can be seen that using the average of equation (17-5), which is the scaling coefficient of the average bending stiffness of the column, ring rib, and wind-resistant ring, combined with equations (16-2), (16-3), (16-4) or their average, to predict the natural frequency of the gasholder body prototype, has a smaller error compared to using other parameters, with a maximum error of 1.130%. When predicting the free vibration frequency of the gasholder body, the natural frequency of the gasholder body prototype can be predicted more accurately by using the scaling coefficient of the average bending stiffness of column, ring rib, and wind-resistant ring in the scaling principle relation.

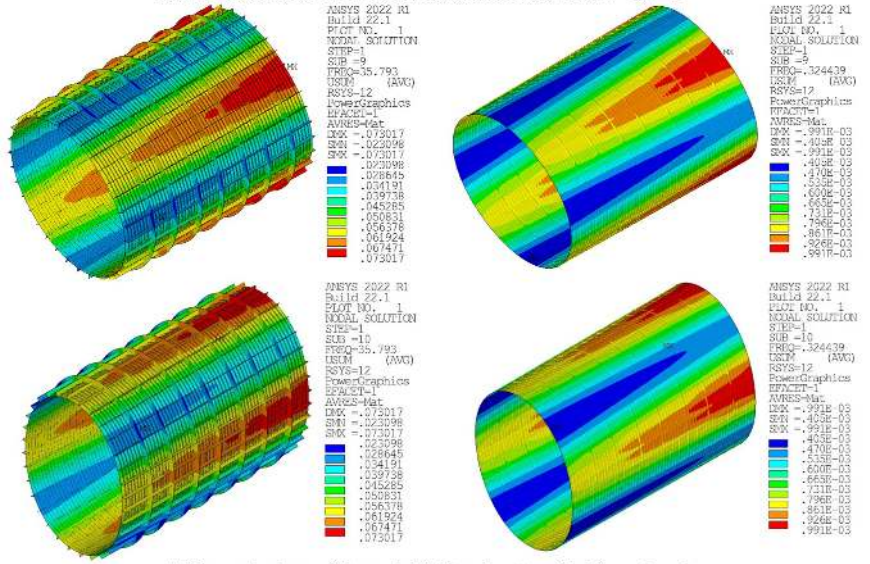
Table 5. Errors between the predicted finite element first-order natural frequency of the gasholder body scaled model with only geometric distortion and the prototype results.

$C_{\bar{M}}$	Errors (%)						
	Equation (17-1)	Equation (17-2)	Equation (17-3)	Equation (17-4)	Equation (17-5)	The average of equation (17-5)	The average of equation (17)
Equation (16-1)	-75.699	1642.753	418.329	196.238	118.641	534.617	841.339
Equation (16-2)	-55.744	177.718	-17.401	-49.209	9.623	**-0.118**	48.157
Equation (16-3)	-56.290	174.291	-18.421	-49.835	10.993	**1.130**	50.008
Equation (16-4)	-55.761	177.610	-17.433	-49.228	10.949	**1.091**	49.949
The average of equation (16-2)~(16-4)	-55.934	176.527	-17.756	-49.427	10.302	**0.501**	49.364
The average of equation (16)	-49.329	217.973	-5.429	-41.847	-12.675	-8.046	71.751

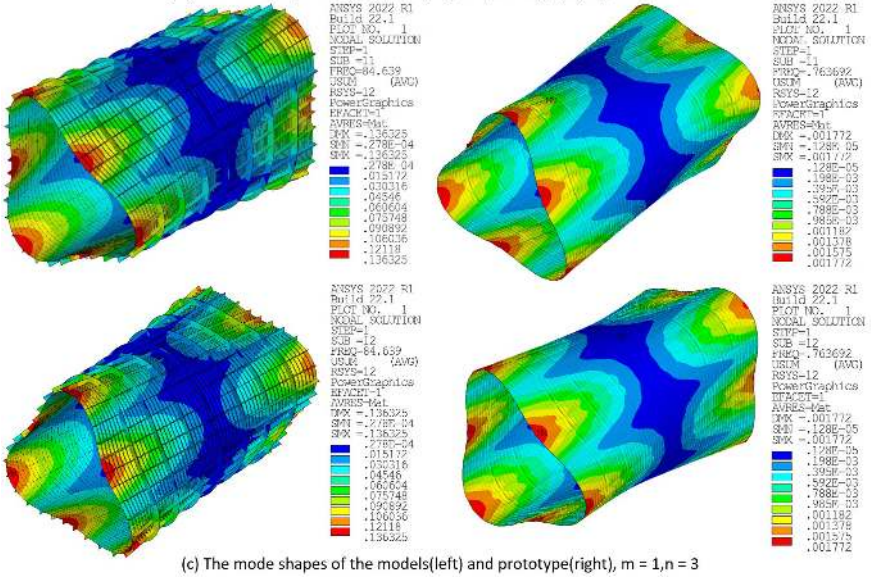
Note: Error = (predicted by FEM results of scaled model - FEM result of prototype) / FEM result of prototype; The first-order vibration mode wave numbers of the gasholder body scaled model with geometric distortion and the prototype are both (1,2).



(a) The mode shapes of the models(left) and prototype(right), m = 1,n = 2



(b) The mode shapes of the models(left) and prototype(right), m = 0,n = 2



(c) The mode shapes of the models(left) and prototype(right), m = 1,n = 3

Fig 7. Comparison of the first-three-order model shapes of the gasholder body scaled model with same materials and only geometric distortion and the prototype.

5.2 Free vibration similarity prediction with both material and geometric dimension distortion

Sometimes, replacement of the material for the test model is typically employed for reasons such as fabrication restrictions, limitations of the test apparatus, changes in the test conditions, cheaper materials, etc. So it is necessary to study the scaled model design method and the scaling principle relation of the free vibration of the longitudinal ring-stiffened cylindrical gasholder body with both material and geometric distortion.

Table 6 presents the first-three-order modal wave numbers and natural frequencies of the free vibration finite element result of the gasholder body prototype, the prototype natural frequency predicted by applying the scaling principle relation (19) based on the natural frequency of the scaled model with both material and geometric distortion, and the error in natural frequency of the predictive prototype and the prototype. Where, C_{sti} of the scaling principle relation (19) is taken as the scaling coefficient of the average bending stiffness of the column, ring rib, and wind-resistant ring in equation (17-5), that is, $C_{\mathrm{sti}} = C_{E_{\mathrm{average}}} C_{I_{0_{\mathrm{average}}}}$, so $C_{\mathrm{sti}} = 26602.154$; $C_{\bar{M}}$ is taken as the scaling coefficient of the average mass value of the column, ring rib, and wind-resistant ring in equations (16-2)~(16-4), and is calculated as $C_{\bar{M}} = 134.438$. Fig 8 shows the first-three-order model shape diagrams of the gasholder body scaled model with both material and geometric distortion as calculated by finite element method and the gasholder body prototype. As can be seen from Table 6 and Fig 8, with both material and geometric distortion, the scaling coefficient adopts the average bending stiffness and mass value of the column, ring rib, and wind-resistant ring, the error between the finite element predicted natural frequency of the gasholder body prototype and the finite element result of the prototype is within 2%, and the finite element free vibration modal wave number of the gasholder body scaled model is the same as that of the prototype; Because the free vibration test of the gasholder body scaled model with both material and geometric distortion can not identify the second-order frequency. The possible reason is that the model structure is relatively large, the energy provided by the hammering method is insufficient to excite all modes, and the time signals that can be captured by the instrument are short, so that some frequencies cannot be identified. Therefore, only the predicted values of the first- and third-order gasholder body prototype natural frequency tests are compared with the prototype finite element results, and the errors are -3.693% and 3.995%, respectively; The above analysis indicates that the free vibration characteristics of the gasholder body scaled model with both material and geometric dimension distortion, combined with the scaling principle relation (19) and relation (20), can well predict the free vibration characteristics of the gasholder body prototype, which fully verifies the correctness of the design method of the gasholder body scaled model with both material and geometric distortion and the free vibration scaling principle relation.

Table 6. Similarity prediction of gasholder body free vibration with both material and geometric dimension distortion.

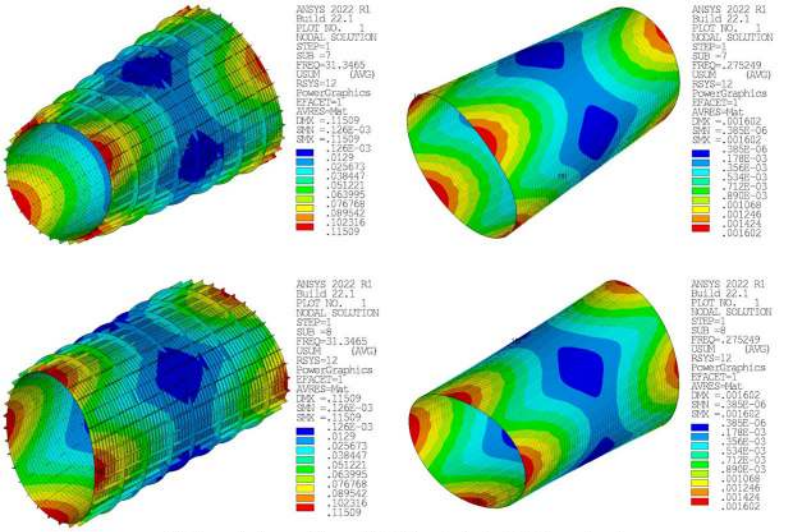
Mode number (*m*,*n*)	Natural frequency calculated by FEM result for the prototype (Hz)	Natural frequency of prototype predicted by FEM results of scaled model (Hz)	Natural frequency of prototype predicted by vibration test results of scaled model (Hz)	Errors[1] (%)	Errors[2] (%)
(1,2)	0.275	0.276	0.265	0.217	-3.693
(1,2)	0.275	0.276	0.265	0.217	-3.693
(0,3)	0.324	0.320	-	-1.334	-
(0,3)	0.324	0.320	-	-1.334	-
(1,3)	0.764	0.763	0.795	-0.038	3.995
(1,3)	0.764	0.763	0.795	-0.038	3.995

Note: Errors[1] = (predicted by FEM results of scaled model - FEM result of prototype) / FEM result of prototype, Errors[2] = (predicted by vibration test results of scaled model - FEM result of prototype) / FEM result of prototype.

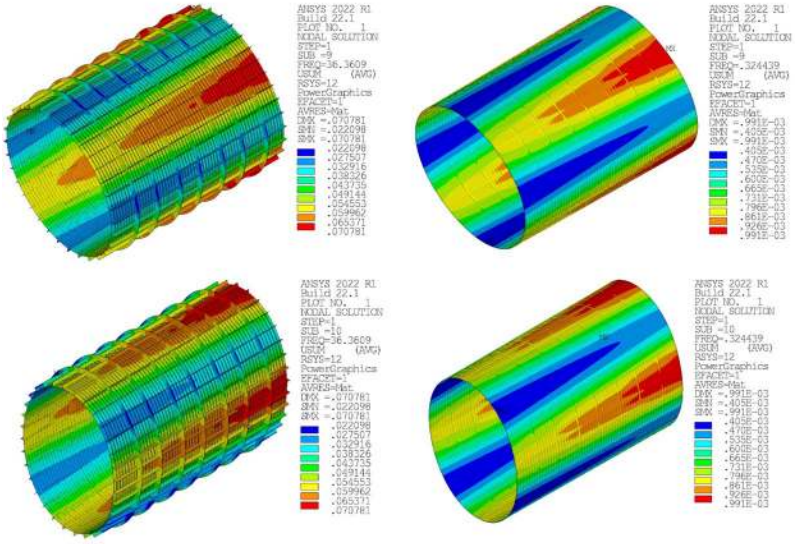
Table 7. Errors between the predicted finite element first-order natural frequency of the gasholder body scaled model with both material and geometric dimension distortion and the prototype results.

$C_{\bar{M}}$	Errors (%)						
	Equation (17-1)	Equation (17-2)	Equation (17-3)	Equation (17-4)	Equation (17-5)	The average of equation (17-5)	The average of equation (17)
Equation (16-1)	-91.484	1732.878	386.185	4.166	89.978	529.591	1662.210
Equation (16-2)	-53.526	191.967	-22.611	-82.221	10.725	**-1.783**	54.150
Equation (16-3)	-54.098	188.161	-23.563	-82.440	11.936	**0.066**	57.053
Equation (16-4)	-53.542	191.648	-22.638	-82.208	12.065	**-0.094**	56.802
The average of equation (16-2)~(16-4)	-46.769	234.170	-11.359	-79.636	10.847	**-0.908**	55.985
The average of equation (16)	-46.850	233.659	-11.494	28.207	-13.780	-8.591	79.881

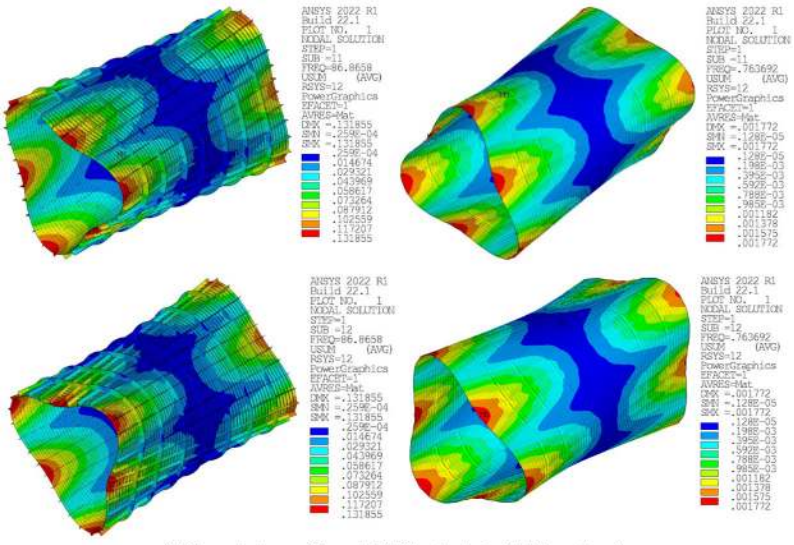
Note: Errors = (predicted by FEM results of scaled model - FEM result of prototype) / FEM result of prototype; The first-order vibration mode wave numbers of the gasholder body scaled model with both material and geometric dimension distortion and the prototype are both (1,2).



(a) The mode shapes of the models(left) and prototype(right), m = 1,n = 2



(b) The mode shapes of the models(left) and prototype(right), m = 0,n = 2



(c) The mode shapes of the models(left) and prototype(right), m = 1,n = 3

Fig 8. Comparison of the first-three-order model shapes of the gasholder body scaled model with both material and geometric dimension distortion and the prototype.

Table 8. Comparison between prototype measured and predicted results of free vibration frequency f/HZ of stiffened cylindrical shell.

Mode no.	Prototype frequency by test (Torkamani et al., 2009)	Model frequency by test (Torkamani et al., 2009)	Prototype frequency by similarity	Errors (%)
1	20.822	61.873	21.554	3.516
2	35.596	109.886	38.280	7.542
3	57.269	163.059	56.804	-0.813
4	62.911	190.099	66.223	5.266
5	91.784	272.047	94.771	3.254
6	100.519	301.168	104.916	4.374

Note: alloy steel: E = 206Gpa, ρ = 7850kg/m^3; aluminum alloy: E = 69Gpa, ρ = 2740kg/m^3; Geometric parameters of the structure can be referred to Reference (Torkamani et al., 2009); Errors = (Prototype frequency by similarity - Prototype frequency by test) / Prototype frequency by test.

Table 7 shows the errors between the predicted first-order natural frequency of free vibration of the gasholder body scaled model with both material and geometric distortion and the prototype finite element results when the coefficients in scaling principle relation (19) are calculated using the equations (16-1)~(16-4), the average values of equations (16-2)~(16-4) and the average values of equations (16), as well as the equations (17-1)~(17-5), the average values of equations (17) and (17-5), respectively. Similarly, only the result with the smallest error in each case is given. By comparison, it can be seen that using the average of equation (17-5), which is the scaling coefficient of the average bending stiffness of the column, ring rib, and wind-resistant ring, combined with equations (16-2), (16-3), (16-4) or their average, the errors between the predicted value of the natural frequency of the gasholder body prototype and the finite element calculation results of the prototype is smaller, with a maximum error of -1.783%. When predicting the free vibration frequency of the gasholder body prototype with the gasholder body scaled model with both material and geometric distortion, the natural frequency of the gasholder body prototype can be predicted more accurately by using the scaling coefficient of the average bending stiffness of the column, ring rib, and wind-resistant ring in the scaling principle relation.

Table 8 shows the comparison between the predicted values of the prototype and the measured values obtained by using the average bending stiffness and mass values in the scaling principle equation (19) when the materials and stiffened rib section forms of the prototype and model are different, and the maximum relative error is 7.542%. Combined with the test data of longitudinal ring-stiffened cylindrical shell in the existing literature, the correctness of scaling principle relation (19) proposed in this paper can be well verified.

6 CONCLUSIONS

In this paper, the longitudinal ring-stiffened cylindrical gasholder body is taken as the research object. According to the discrete reinforcement theory and energy method, the generalized similarity condition and the scaling principle relation of its free vibration were derived directly from the total energy of the gasholder body. On this basis, a distortion similarity design method of gasholder body free vibration scaled model is proposed and the scale model with geometric distortion and geometric and material distortion is designed and manufactured. By using the finite element method and test method, and combined with the relation of free vibration scaling principle derived from theory, the free vibration similarity prediction of longitudinal ring-stiffened cylindrical gasholder body with geometric distortion and with both material and geometric distortion is carried out. The following conclusions are drawn:

1. By comparing with the examples in the literature, the accuracy of the finite element free vibration analysis is guaranteed; By comparing the finite element free vibration results of the gasholder body scaled model with the results of the free vibration test, the reliability of the free vibration test is also ensured.

2. Finite element analysis and test results of the gasholder body scaled model with only geometric distortion, combined with the scaling coefficient of the average bending stiffness of the column, ring rib, and wind-resistant ring as well as the scaling coefficient of the average mass value, can accurately predict the free vibration characteristics of the gasholder body prototype. Moreover, the accuracy and feasibility of the design method for achieving geometric distortion of the gasholder body free vibration scaled model using the equivalent tension-compression stiffness and bending stiffness of the stiffened ribs are verified.

3. Finite element analysis and test results of the gasholder body scaled model with both material and geometric distortion, combined with the scaling coefficient of the average bending stiffness of the column, ring rib, and wind-resistant ring as well as the scaling coefficient of the average mass value, can accurately predict the natural frequency of the gasholder body prototype, with the error within 4%. It can be seen from Tables 5 and 7 that the errors predicted using the average of Eqs. (16) and (17) (i.e., the average of the mass and the different stiffnesses of the skin and the stiffened ribs) are larger for both the geometrically distorted and scaled model with both material and geometric distortion. At the same time, it has been proven that, based on geometric distortion, considering the material distortion of the scaled model, and using the equivalent tension-compression stiffness and bending stiffness of the skin and stiffened rib, the design and production of the gasholder body scaled model with both material and geometric distortion can be achieved.
4. The proposed design method for gasholder body scaled model with geometric distortion and both material and geometric uniform distortion, and the derived relation for gasholder body free vibration scaling principle are accurate, reliable, and easy to use, which can provide reference for the design, test, and similarity prediction of dynamic scaled models with distortion for similar large general longitudinal ring-stiffened cylindrical structures.
5. This manuscript only uses a set of scale factors, and does not use multiple sets of scale factors for verification. The derived scaling principle relation is the condition that the complete similarity between the prototype and the scale model needs to be satisfied. For scale models with different materials, equation (14) is not completely true, but it can be predicted by equation (19) of scale principle.
6. Due to insufficient experimental equipment conditions currently, the frequency response function has not been measured in the free vibration test, making it impossible to compare the free vibration mode results of the gasholder body finite element method and the test. In addition, based on the discrete stiffening theory and the total energy of the structural system, further design and similarity prediction of the scaled model with distortion can be carried out on the forced vibration of the gasholder body.

ACKNOWLEDGEMENTS

This work is supported by the National Natural Science Foundation of China (Grant No. 51868013, 52068015), Doctoral Research Initiation Fund of Guilin University of Technology (GUTQDJJ2017034) and Guangxi Key Laboratory of Green Building Materials and Construction Industrialization (No. 22-J-21-13). The authors are grateful for these financial supports.

Author's Contribuitions: Conceptualization, Ce Zheng and Wei Yu; Methodology, Ce Zheng, Wei Yu; Investigation, Ce Zheng, Wei Yu, Shihao Chen; Writing - original draft, Ce Zheng, Wei Yu; Writing - review & editing, Wei Yu; Funding acquisition, Wei Yu, Yanguo Yang; Project administration, Wei Yu; Data curation, Ce Zheng; Formal analysis, Ce Zheng, Wei Yu; Validation, Ce Zheng; Visualization, Ce Zheng, Wei Yu; Resources, Wei Yu, Lu Zhang, Shenghua Zhao; Supervision, Wei Yu.

Editor: Marcílio Alves

References

Amabili, M. (2008). Nonlinear vibrations and stability of shells and plates, Cambridge University Press, 29-32.

Chen, J. (2001). Stability of steel structures theory and design. Beijing: Science Press, 209-210.

Cohen, T.C., Diu, B., Laloe, F. (1977). Quantum Mechanics, Volume II. New York: Wiley Press, 1469-1471.

Egle, D.M., Sewall, J.L. (1968). An analysis of free vibration of orthogonally stiffened cylindrical shells with stiffeners treated as discrete elements. AIAA Journal, 6(3): 518-526.

Fisher, C.A. (1972). Dynamic buckling of an axially compressed cylindrical shell with discrete rings and stringers, Ph.D. The University of Oklahoma Graduate College, Oklahoma.

Golchi, M., Talebitooti, M., Talebitooti, R. (2019). Thermal buckling and free vibration of FG truncated conical shells with stringer and ring stiffeners using differential quadrature method. Mechanics Based Design of Structures and Machines, 47(3): 255-282.

Institute of Mechanics, Chinese Academy of Sciences, Group of Solid Mechanics Research Shell. (1983). Stiffened cylindrical panels and cylindrical shells. Beijing: Science Press, 15-17.

Jafari, A.A. and Bagheri, M. (2006) Free vibration of non-uniformly ring stiffened cylindrical shells using analytical, experimental and numerical methods. Thin-Walled Structures, 44(1): 82-90.

Jam, J., Zadeh, M., Taghavian, H., Eftari, B. (2012). Vibration analysis of grid-stiffened circular cylindrical shells with full free edges. Polish Maritime Research, 18(4): 23-27.

Lee, Y.S., Kim, Y.W. (1998). Vibration analysis of rotating composite cylindrical shells with orthogonal stiffeners. Computers & Structures, 69(2): 271-281.

Li, Z.L., Wang, J.C., Yu, W., Zhu, W.X. (2022). Study on post-buckling scale model of stringer stiffened-cylindrical shells under axial compression based on discrete stiffened method. Journal of Hunan University (Natural Sciences), 49(03): 123-132.

Liu, C., Liu, W.G., Liu, Z.P. (2021). Effects of inner ring-stiffener on modal frequencies of a functionally graded cylindrical shell. Journal of Vibrational and Shock, 40(24): 255-262.

Liu, L., Cao, D, Sun, S. (2013). Vibration analysis for rotating ring-stiffened cylindrical shells with arbitrary boundary conditions. Journal of Vibration and Acoustics, 135(6): 061010.

Liu, L., Cao, D.Q., Sun, S.P., Gang, L. (2016). Vibration analysis of orthogonal stiffened cylindrical shells constrained by elastic boundary. Journal of Ship Mechanics, 20(08): 1016-1027.

Luo, Z., Wang, Y., Zhu, Y., Wang, D.Y. (2016). The dynamic similitude design method of thin walled structures and experimental validation. Shock and Vibration, 2016.

Mustafa, B. A. J., Ali, R. (1989). An energy method for free vibration analysis of stiffened circular cylindrical shells. Computers & structures, 32(2): 355-363.

Niu, N., Sun, L.L., Xing, Z.Z., Zhao, G.D., Wang, X.H., Wu, Y.Y. (2023). Calculation and analysis of inherent properties of stiffened cylindrical shells with longitudinal stiffeners of arbitrary cross section under typical boundary conditions. Journal of Vibration Engineering, 36(01): 96-106.

Rinehart, S.A. and Wang, J.T.S. (1972). Vibration of simply supported cylindrical shells with longitudinal stiffeners. Journal of Sound and Vibration, 24 (2): 151-163.

Torkamani, S., Navazi, H.M., Jafari, A.A., Bagheri, M. (2009). Structural similitude in free vibration of orthogonally stiffened cylindrical shells. Thin-Walled Structures, 47(11): 1316-1330.

Ungbhakorn, V., Singhatanadgid P. (2009). A scaling law for vibration response of laminated doubly curved shallow shells by energy approach. Mechanics of Advanced Materials and Structures, 16(5): 333-344.

Wang, Y., Yu X.G., Luo, Z., Xie, Z.W. (2018). Travelling wave resonance characteristics of a high-speed rotating thin short cylindrical shell with sealing teeth in various boundary conditions. Journal of Vibrational and Shock, 37(10): 20-26+56.

Yu, W. and Li, Z.L. (2016). Structural similitude for prestressed vibration and buckling of eccentrically stiffened circular cylindrical panels and shells by energy approach. International Journal of Structural Stability and Dynamics, 16(10): 1550074.

Zhou, L.L., Li, D.K. (2019). Design of scaled model for dynamic characteristics of stiffened cylindrical shells based on equivalent similar method. The Aeronautical Journal, 123(1261): 398-415.

Nomenclature

A	cross-sectional area of stiffener
B	extensional rigidity
b	long side of rectangular stiffened rib
b_f	length of stiffened rib flange
D	bending rigidity
d	spacing between two stiffened ribs
E	Young's modulus
e	distance from the centroid of stiffened rib to the middle surface of skin
f	natural frequency
G	shear modulus
h	thickness of gasholder body skin
h_w	length of stiffened rib web
I_0	moments of inertia from stiffened rib to the middle surface of skin
J	torsion constants of stiffened rib
L	height of gasholder body
$\bar{M}$	mass per unit area
m	longitudinal half wave number
n_i	starting numbers of each ring rib and each wind-resistant ring
N_i	ending numbers of each ring rib and each wind-resistant ring
n	circumferential wave number
n_0	rectangular number of stiffened rib section
R	radius of gasholder body
T	kinetic energy
t	short side of rectangular stiffened rib
t_f	thickness of stiffened rib flange
t_w	thickness of stiffened rib web
U	strain energy
u	gasholder body skin displacement in the x direction
v	gasholder body skin displacement in the y direction
w	gasholder body skin displacement in the z direction
ε	strains in the middle surface of gasholder body skin
χ	curvatures of gasholder body skin
μ	Poisson's ratio of the skin material
ρ	mass density
Ω	circular frequency
Π	total energy of the structural system
δ	Dirac delta function

Subscripts

c	gasholder body skin
k	wind-resistant ring
m	model
p	prototype
r	ring rib
s	longitudinal rib
sti	stiffness